Acta Crystallographica Section F
Structural Biology and Crystallization Communications
ISSN 1744-3091

The structure of PhaZ7 at atomic (1.2 Å) resolution reveals details of the active site and suggests a substrate-binding mode

Sachin Wakadkar,[a] Siska Hermawan,[b] Dieter Jendrossek[b] and Anastassios C. Papageorgiou[a]*

[a]Turku Centre for Biotechnology, University of Turku and Åbo Akademi University, Finland, and [b]Institute for Microbiology, University of Stuttgart, Germany

Correspondence e-mail: tassos.papageorgiou@btk.fi

Received 2 March 2010
Accepted 19 April 2010

PDB References: PhaZ7–SO_2 complex, 2x5x; free PhaZ7, 2x76.

Poly-(*R*)-hydroxyalkanoates (PHAs) are bacterial polyesters that are degraded by a group of enzymes known as PHA depolymerases. *Paucimonas lemoignei* PhaZ7 depolymerase is the only extracellular depolymerase that has been described as being active towards amorphous PHAs. A previously determined crystal structure of PhaZ7 revealed an α/β-hydrolase fold and a Ser-His-Asp catalytic triad. In order to address questions regarding the catalytic mechanism and substrate binding, the atomic resolution structure of PhaZ7 was determined after cocrystallization with the protease inhibitor PMSF. The reported structure has the highest resolution (1.2 Å) of currently known depolymerase structures and shows a sulfur dioxide molecule covalently attached to the active-site residue Ser136. Structural comparison with the free PhaZ7 structure (1.45 Å resolution) revealed no major changes in the active site, suggesting a preformed catalytic triad. The oxyanion hole was found to be formed by the amide groups of Met137 and Asn49. Nine well ordered water molecules were located in the active site. Manual docking of a substrate trimer showed that the positions of these water molecules coincide well with the substrate atoms. It is proposed that these water molecules are displaced upon binding of the substrate. Furthermore, conformational changes were identified after comparison with a previously determined PhaZ7 dimer structure in a different space group. The changes were located in surface loops involved in dimer formation, indicating some flexibility of these loops and their possible involvement in polyester binding.

1. Introduction

Many bacteria store carbon and energy in the form of poly-(*R*)-hydroxyalkanoates (PHAs) during unbalanced growth conditions such as the absence of nitrogen and the presence of excess carbon. PHAs form inclusion bodies intracellularly (i-PHAs) and constitute up to 90% of the cellular dry weight (Madison & Huisman, 1999; Jendrossek, 2009). PHAs are also found in extracellular environments (e-PHAs). Poly-(*R*)-hydroxybutyric acid (PHB) is the most commonly found polyester in bacteria. The bacterial copolymer poly(3HB-co-3HV), which is composed of (*R*)-3-hydroxybutyric acid and (*R*)-3-hydroxyvaleric acid, has been commercialized under the name Biopol (Jendrossek & Handrick, 2002). Moreover, several companies from different countries offer a growing range of microbially produced PHAs (Biopol, Mirel, Enmat, Nodax, Biocycle and Biomer).

PHAs have been classified on the basis of the number of C atoms in the monomer as short-chain-length PHAs (PHA_{SCL}; 3–5 C atoms) and medium-chain-length PHAs (PHA_{MCL}; six or more C atoms) (Jendrossek & Handrick, 2002). They can consist of only one hydroxyalkanoic acid (homopolymers) or of several different hydroxyalkanoic acids (copolymers) from a variety of around 150 different hydroxyalkanoic acids (Steinbüchel & Valentin, 1995). PHAs show different physical and chemical properties depending on the composition and number of different monomers (Jendrossek & Handrick, 2002; Jendrossek, 2009). Importantly, PHAs are degraded to water-soluble compounds by a group of enzymes known as PHA depolymerases that are secreted by bacteria and fungi. PHA de-

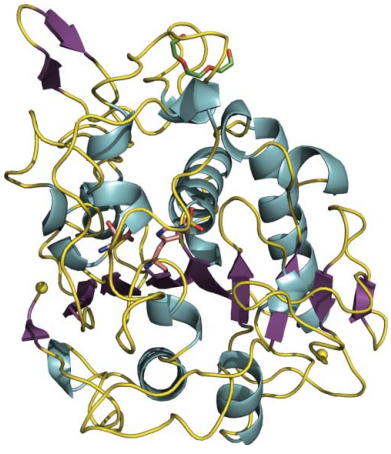

polymerases have been classified as either i-PHA depolymerases or e-PHA depolymerases depending on their ability to degrade the respective forms of PHAs (Jendrossek, 1998).

Although e-PHAs and i-PHAs are chemically the same, microbes treat them differently. i-PHAs, which are amorphous in nature and are considered to be the native (nPHA) form of the polyester, are accumulated by bacteria themselves and are covered by a surface composed mainly of proteins. In the absence of an exogenous carbon source, the survival of bacteria depends on i-PHAs. Accordingly, the degradation of i-PHAs is termed an active mobilization owing to the use of indigenous carbon. In contrast, e-PHAs are produced as the result of cell death. They remain present in a partially crystallized form that contains an amorphous fraction within it and are considered to be the denatured (dPHA) form. e-PHAs are used as an extracellular source of carbon by bacteria; therefore, their degradation is termed as the utilization of exogenous carbon (Jendrossek *et al.*, 1996; Pötter & Steinbüchel, 2005). Hence, similar notation is used (nPHA depolymerases or dPHA depolymerases) to represent PHA depolymerases that degrade the respective forms of PHAs (Jendrossek & Handrick, 2002).

Although some progress has been made since 2002, there is still little information about i-PHA depolymerases (Abe *et al.*, 2005; Chen *et al.*, 2009). In contrast, more than 50 e-PHA depolymerases from different microorganisms, such as Gram-negative aerobic bacteria, Gram-positive aerobic bacteria and fungi, have been purified and characterized. All characterized e-PHA depolymerases specifically act on crystalline PHA_{SCL} or PHA_{MCL} and are inactive against nPHAs (Jendrossek, 2002). Functional analysis of e-PHA_{SCL} depolymerases shows that all depolymerases have a complex multi-domain structure.

Of PHA-degrading bacteria, *Paucimonas lemoignei* and *Ralstonia pickettii* T1 have been the most studied (Saito *et al.*, 1989; Hiraishi *et al.*, 2006). *P. lemoignei* secretes at least seven different e-PHA depolymerases: PhaZ1–PhaZ7. The first six depolymerases (PhaZ1–PhaZ6) are active against dPHB, whereas PhaZ7 is active against the amorphous form, mainly nPHB (Handrick *et al.*, 2001; Reinhardt *et al.*, 2002). Accordingly, the first six depolymerases are termed e-dPHA depolymerases, whereas PhaZ7 is termed an e-nPHA depolymerase (Jendrossek, 2001).

PhaZ7 consists of a single domain and exhibits no sequence similarity to any of the other e-PHA depolymerases apart from the so-called lipase box (Jendrossek & Handrick, 2002). As a single-domain protein, PhaZ7 shows a resemblance to *Penicillium funiculosum* e-PHB depolymerase, which also contains a single domain (Papageorgiou *et al.*, 2008; Miyazaki *et al.*, 2002; Hisano *et al.*, 2006). Additionally, both depolymerases catalyze similar reactions, act as serine hydrolases based on a Ser-Asp-His catalytic triad and have an α/β-fold. The crystal structures of PhaZ7 and *Pe. funiculosum* e-PHB depolymerase have been determined previously (Papageorgiou *et al.*, 2008; Hisano *et al.*, 2006). Moreover, the crystal structure of the poly(3-hydroxybutyrate) depolymerase Lpqc from *Bordetella parapertussis*, a putative intracellular PHB depolymerase, has recently been determined at 1.83 Å resolution (PDB code 3d0k; Y. Kim, C. Tesar, R. Jedrzejczak & A. Joachimiak, unpublished work).

In order to obtain further information about the catalytic mechanism, the interaction with the substrate and the conformational changes during catalysis, structural studies of PhaZ7 with the serine protease inhibitor phenylmethylsulfonyl fluoride (PMSF) were undertaken. Crystal structures of PhaZ7 were determined at 1.20 and 1.45 Å resolution. The results revealed the binding of a sulfur dioxide molecule at the active site (hereafter referred to as the PhaZ7–SO_2 structure), which allowed detailed characterization of the interactions with the catalytic triad residues. Furthermore, comparison with the free PhaZ7 structure (Papageorgiou *et al.*, 2008) revealed conformational changes in surface loops, suggesting a potential site and mechanism for biopolymer binding. The high resolution of the structure also allowed a detailed mapping of the active-site architecture and clear localization of the water molecules in its vicinity.

2. Methods

2.1. Isolation and purification of PhaZ7

PhaZ7 was isolated and purified from a *P. lemoignei* culture grown on succinate. After 80 h of growth, the culture was harvested by centrifugation. The cell-free culture fluid was concentrated by ultrafiltration followed by ammonium sulfate (85% saturated) precipitation. The PhaZ7-containing precipitate was dissolved and eluted with a 0–200 m*M* NaCl gradient on a CM-Sepharose CL-6B column. The PhaZ7-containing fractions from the column were pooled and subsequently applied onto a Mono-P column. Elution was carried out using Pharmalyte polybuffer (Amersham Pharmacia). Pharmalyte was subsequently removed by gel filtration. PhaZ7 was found to be 98% pure as confirmed by SDS–PAGE. All steps were performed at room temperature. The use of room temperature instead of 277 K during purification and the removal of Pharmalyte were the only modifications of the original protocol used in previous crystallizations of PhaZ7 (Handrick *et al.*, 2001; Kapetaniou *et al.*, 2005). The concentration of purified PhaZ7 was determined spectroscopically with a Nanodrop 2000c spectrophotometer by measuring the absorbance at 280 nm using a molar absorption coefficient (ε) of 0.73 for 1.0 mg ml^{-1}. The protein was concentrated to 4.5 mg ml^{-1} in 10 m*M* Tris–HCl pH 8.5 buffer and stored at 277 K prior to crystallization.

2.2. Crystallization of PhaZ7

PhaZ7 was crystallized in the free form and in the presence of PMSF using the hanging-drop vapour-diffusion method at 289 K. The well solution consisted of 20%(*w*/*v*) PEG 3350 and 0.2 *M* sodium iodide. 1.5 µl protein solution was mixed with an equal volume of well solution on siliconized cover slips. For cocrystallization, a 0.1 *M* PMSF stock solution in 2-propanol was added to the well to a final concentration of 10 m*M*. Crystals appeared after 1 d and reached their final size within 3 d.

2.3. Data collection

Data were collected to 1.2 and 1.45 Å resolution for the PhaZ7–SO_2 complex and free PhaZ7, respectively, on the ID14-2 beamline (λ = 0.9330 Å) at the European Synchrotron Radiation Facility (ESRF), Grenoble, France. Prior to data collection, single crystals were soaked for a few seconds in reservoir solution supplemented with 20%(*w*/*v*) glycerol as a cryoprotectant. The crystals were subsequently flash-cooled to 100 K using a liquid-nitrogen stream. A total of 150 images were collected for each data set with 1.0° rotation and an exposure time of 4 s per image. The diffraction data were recorded on an Area Detector Systems Corporation (ADSC) Quantum 4 charge-coupled device detector and were subsequently processed using the *XDS* suite (Kabsch, 2010). The crystals were found to belong to space group $P2_12_12$, with unit-cell parameters $a = 49.6$, $b = 140.6$, $c = 56.7$ Å and one molecule in the crystallographic asymmetric unit.

2.4. Structure determination and refinement

Initial phases were determined by the molecular-replacement method using the program *Phaser* (McCoy *et al.*, 2007) with the structure of PhaZ7 determined previously in a centred monoclinic (*C*2) space group as the search model (Papageorgiou *et al.*, 2008).

For PhaZ7–SO_2, initial refinement was carried out using *REFMAC* (Murshudov *et al.*, 1997). A test set composed of 5% of the total reflections assigned at random was excluded from refinement to allow the calculation of R_{free}. Water molecules were initially added to the structure by using the automatic procedure available in *REFMAC*. In the later stages of refinement the program *SHELX*-97 (Sheldrick, 2008) was employed. Four rounds of isotropic refinement were initially performed in *SHELX*-97 followed by several rounds of anisotropic refinement. After the first anisotropic refinement, R_{free} fell from 25.3% to 19.6%. In contrast, isotropic refinement slightly reduced R_{free} to 25.2%, thus confirming the use of anisotropic refinement as a better strategy for refinement of the structure.

In the case of the free PhaZ7 structure refinement was carried out in *SHELX*-97. 19 rounds of isotropic refinement were initially performed followed by several rounds of anisotropic refinement that lowered R_{free} from 22.5% to 19.2% in the first round.

Water molecules were automatically added to the structures by *SHELX*-97. The program *Coot* (Emsley & Cowtan, 2004) was employed for rebuilding and visualization of the structures. Both structures were validated using *PROCHECK* from the *CCP*4 suite (Collaborative Computational Project, Number 4, 1994) and the tools available in *Coot* (Emsley & Cowtan, 2004). Structural superposition was carried out by the program *SUPERPOSE* from the *CCP*4 program suite (Krissinel & Henrick, 2004). Data-collection and refinement statistics are given in Table 1.

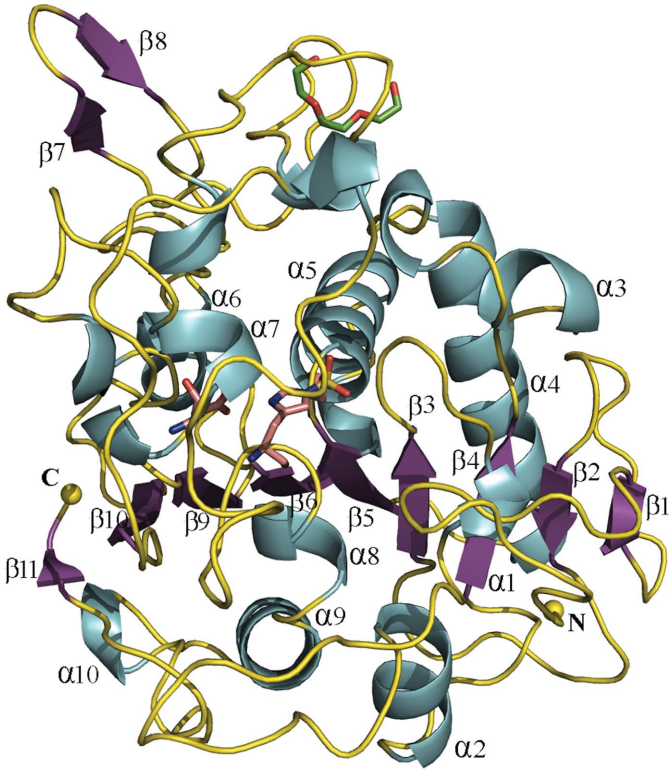

Figure 1
Cartoon diagram of the PhaZ7–SO_2 complex. α-Helices are shown in cyan and β-strands are shown in magenta. The N- and C-termini are shown as yellow spheres. The bound SO_2 and the catalytic triad (Ser136, Asp242 and His306) are depicted as yellow and salmon sticks, respectively. The PEG fraction is shown as green sticks. Secondary-structure elements were assigned according to *PDBsum* (http://www.ebi.ac.uk/thornton-srv/databases/pdbsum).

Table 1
Data-collection and refinement statistics.

Values in parentheses are for the highest resolution shell.

	PhaZ7–SO_2	Free PhaZ7
Data collection		
Beamline	ESRF ID14-2	ESRF ID14-2
Wavelength (Å)	0.9330	0.9330
Resolution range (Å)	20.0–1.20 (1.23–1.20)	20.0–1.45 (1.49–1.45)
Space group	$P2_12_12$	$P2_12_12$
Unit-cell parameters (Å)	a = 49.6, b = 140.6, c = 56.7	a = 49.8, b = 140.7, c = 56.8
Measured reflections	731249 (51125)	422004 (30925)
Unique reflections	124737 (9116)	71446 (5191)
Completeness (%)	99.9 (99.9)	99.9 (99.8)
R_{merge}† (%)	9.9 (43.1)	9.5 (43.4)
R_{meas}‡ (%)	10.8 (47.4)	10.4 (47.5)
$\langle I/\sigma(I)\rangle$	11.1 (3.6)	13.1 (4.1)
Mosaicity (°)	0.21	0.24
Wilson B factor (Å^2)	12.8	15.5
Refinement statistics		
Resolution range (Å)	20.0–1.20	20.0–1.45
Reflections (working/test)	118436/6235	67830/3564
R_{cryst}/R_{free}§ (%)	13.9/17.6	13.4/17.8
Protein atoms	2612	2602
Water molecules	563	470
SO_2	1	—
I^-	8	8
Cl^-	6	6
Na^+	2	2
PG4¶	1	—
GOL	—	1
R.m.s.d.		
Bond lengths (Å)	0.011	0.009
Bond angles (°)	1.80	1.72
Average B factors (Å^2)		
All atoms	14.6	13.3
Main chain	9.4	9.5
Side chain	11.8	11.9
Waters	32.8	27.3
SO_2	15.3	—
I^-	23.4	27.2
Cl^-	18.2	22.0
Na^+	12.2	10.1
PG4¶	30.9	
GOL	—	32.2
Ramachandran plot (%)		
Most favoured regions	86.9	85.5
Additionally allowed region	12.4	13.8
Generally allowed region	0.7	0.7
Disallowed region	0	0

† $R_{merge} = \sum_{hkl}\sum_i |I_i(hkl) - \langle I(hkl)\rangle| / \sum_{hkl}\sum_i I_i(hkl)$, where $I_i(hkl)$ is the ith observation of reflection hkl and $\langle I(hkl)\rangle$ is the weighted average intensity for all observations i of reflection hkl. ‡ R_{meas} (also known as $R_{r.i.m.}$) is the redundancy-independent merging R value (Diederichs & Karplus, 1997). § $R_{cryst} = \sum_{hkl} ||F_{obs}| - |F_{calc}|| / \sum_{hkl} |F_{obs}|$, where F_{obs} and F_{calc} are the observed and calculated structure factors, respectively. For R_{free} calculations, the sum was extended over a subset of reflections (5%) that were randomly selected and omitted from all stages of refinement. ¶ PG4 refers to a fraction of PEG.

3. Results

3.1. Quality of the structures

The crystal structure of PhaZ7–SO_2 was determined to 1.2 Å resolution and that of free PhaZ7 to 1.45 Å resolution. Both structures refined with good geometry and refinement statistics. The refined structure of PhaZ7–SO_2 had R_{cryst} and R_{free} values of 13.9% and 17.6%, respectively. The free PhaZ7 structure had R_{cryst} and R_{free} values of 13.4% and 17.8%, respectively. The overall B factors for the PhaZ7–SO_2 and free PhaZ7 structures were 10.6 and 10.7 Å^2, respectively. The Ramachandran plot shows that no residues from either structure were in the disallowed region. Heteroatoms from the

crystallization buffer solution are present at identical positions in both structures. Iodides, in particular, were identified by an anomalous map calculated using data collected in-house on a rotating-anode generator (λ = 1.5418 Å). Double conformations were found for 16 residues (Thr2, Ser35, Met58, Ser64, Gly67, Arg71, Ser95, Ser96, Ser100, Ser128, Ile132, Met137, Ser192, Ser215, Cys255 and Met291) in the 1.2 Å structure. In the same structure, the coordinate error was 0.03 Å as deduced by the diffraction precision indicator (Cruickshank, 1999). The clashscore is 2.72 (96th percentile) for all atoms as defined by *MolProbity* (Chen *et al.*, 2010). Finally, anisotropy analysis using *PARVATI* showed an anisotropy distribution of 0.347 and a standard deviation of 0.132, which are within the typical ranges found for protein structures (Merritt, 1999).

3.2. Overall structure

PhaZ7 is a single-domain globular protein (342 residues) with approximate dimensions of 50 × 52 × 45 Å (Fig. 1) and an α/β-hydrolase fold (Papageorgiou *et al.*, 2008). The structure consists of 11 β-strands (β1–β11), eight α-helices (α1–α8) and ten 3_{10}-helices ($\alpha1'$–$\alpha10'$). All of the β-strands are present in the core of the structure and form a mixed β-sheet, except for two (β7 and β8) which are present at the surface in an antiparallel fashion. All cysteine residues are involved in disulfide-bridge formation. Thus, five disulfide bridges are present: Cys3–Cys11, Cys36–Cys85, Cys171–Cys184, Cys246–Cys255 and Cys325–Cys330. However, none of them are essential for activity (Handrick *et al.*, 2001). The number of water molecules present in the structures varies according to the resolution, with the atomic resolution structure containing 563 water molecules in total.

In the PhaZ7–SO_2 complex eight iodides, six chlorides and two sodium ions were found at the surface along with a small fraction of PEG composed of four ethylene glycol residues. The PEG fraction was accommodated by replacing four water molecules in a surface cavity formed by the aromatic residues Tyr105, Tyr176, Tyr189 and Tyr190, and Pro182. A SO_2 group from PMSF was found to be present at the active site near the catalytic residue Ser136. In free PhaZ7 a total of eight iodides, six chlorides, two sodium ions and a glycerol molecule were found at the surface of the protein.

3.3. Structural comparison with other depolymerases

Structural comparison using *SSM* (Krissinel & Henrick, 2004) was carried out against *Pe. funiculosum* e-PHB depolymerase (Hisano *et al.*, 2006; PDB code 2d80) and the *B. parapertussis* putative poly-(3-hydroxybutyrate) depolymerase Lpqc (PDB code 3d0k). All three depolymerases are characterized by an α/β-fold, with *Pe. funiculosum* e-PHB depolymerase adopting a circularly permuted α/β-fold instead of a canonical one (Hisano *et al.*, 2006). Despite the overall fold similarity, the r.m.s.d. in C^{α}-atom positions was found to be high: 2.7 (103 residues aligned) and 2.9 Å (176 residues aligned) for 2d80 and 3d0k, respectively. Similarly, the r.m.s.d. between *Pe. funiculosum* e-PHB depolymerase and Lpqc is 2.9 Å for an alignment length of 106 residues. The solvent-accessible surface area (SASA) of PhaZ7 is 11 850 $Å^2$ as calculated by *PISA* (Krissinel & Henrick, 2007). The SASA values for 2d80 and 3d0k are in the same range (11 014 and 12 327 $Å^2$, respectively).

3.4. Analysis of the active site

The active site of PhaZ7 contains a catalytic triad composed of Ser136, His306 and Asp242 found after strands β5, β9 and β10, respectively (Papageorgiou *et al.*, 2008). It is deeply buried inside the structure and forms a small cavity surrounded by Asn49, Ser136, Met137 and His306 on one side, and Ala162, Gly164, Asp242, Val244, Trp287, Phe197, Met291 and Leu168 on the other. The side chains of Met137 and Met291 have been modelled in double conformations. The catalytic triad residues are present in a line at the edge of the cavity. The volume of this cavity is approximately 7 $Å^3$ as measured by *VOIDOO* (Kleywegt & Jones, 1994). The cavity in free PhaZ7 is filled with nine water molecules that are well defined with low *B* factors, most of which are between 15 and 25 $Å^2$.

The spatial arrangement of the catalytic triad residues is similar to that in *Pe. funiculosum* e-PHB depolymerase (Hisano *et al.*, 2006). The corresponding catalytic residues are Ser39, Asp121 and His155. In Lpqc, the catalytic residues Ser145, Asp213 and His268 are found after strands β5, β7 and β8, respectively. They form a crevice at the surface of the enzyme, with Asp213 and His268 being solvent-exposed. Only Ser145 and His268 superimpose well with the corresponding Ser136 and His306 of PhaZ7 (distances of 1.4 and 3.3 Å, respectively, between C^{α} atoms, 2.6 Å between OG atoms and 3.0 Å between ND1 atoms). In contrast, Asp213 is situated about 2.9 Å away in a different location from that of PhaZ7 Asp242 and is closer to Ala238 (distance of ∼1.5 Å in C^{α}-atom positions). The side chain of Asp242 overlaps well with Arg234 of Lspq.

3.5. SO_2 binding

The structure determination of PhaZ7 cocrystallized with PMSF revealed the binding of an SO_2 group in the active site between Ser136 OG and His306 NE2 (Fig. 2). The SO_2 molecule is well defined in the electron-density map (above 12σ for the S atom), with an average *B* factor of 15.6 $Å^2$. Upon SO_2 binding, the O atoms

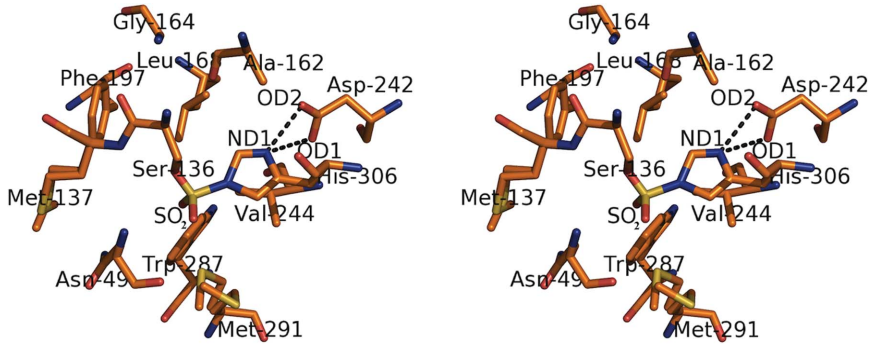

Figure 2
Stereoview of the active site of the PhaZ7–SO_2 complex shown in stick representation. The interactions of the carboxylate group of Asp242 with His306 ND1 are depicted (dashed lines).

replace two water molecules that are present in the free PhaZ7 structure. Furthermore, the catalytic Ser136 OG is slightly displaced (by approximately 0.3 Å) and moves closer to His306 NE2. In contrast, the distance between the carboxylate-group O atoms of Asp242 and His306 ND1 remains the same (3.19 and 2.87 Å). The distances of the S atom of SO_2 from Ser136 OG and His306 NE2 are 1.43 and 1.64 Å, respectively.

Asn49 and Met137 have previously been suggested to be the oxyanion hole-forming residues (Papageorgiou *et al.*, 2008). Indeed, Ser136 OG of PhaZ7 is involved in a hydrogen bond (2.71 Å) to the backbone N atom of the next residue (Met137). In addition, the O2 atom of SO_2 is hydrogen bonded to Asn49 N (3.25 Å). In the absence of SO_2, the distance between Ser136 OG and Met137 N increases by approximately 0.1 Å. Both Met137 and Asn49 were found to be in the same positions as in the free structure, suggesting that no major rearrangements are required for formation of the oxyanion hole.

3.6. Comparison with the 1.9 Å resolution PhaZ7 structure

The refined atomic resolution structure of PhaZ7–SO_2 was compared with the PhaZ7 structure previously determined at 1.9 Å resolution (PDB code 2vtv; Papageorgiou *et al.*, 2008). Secondary-structure comparison revealed a slightly different secondary-structure assignment to that observed in the previous PhaZ7 structure, mainly involving the assignment of Gln243–Cys246 as a short four-residue α-helix in the 1.2 Å structure. As a result, an extra β-α-β motif is created involving β-strands β9 (residues 232–237) and β10 (residues 268–273). Additionally, the Ser170–Thr174 α-helix in the 2vtv structure is transformed into a 3_{10}-helix between Tyr169 and Cys171. To identify additional structural differences that occur in the three-dimensional structure, chain *A* of 2vtv was superimposed onto the PhaZ7–SO_2 structure (Fig. 3). The r.m.s.d. for C^{α} atoms was 0.36 Å. The superimposed structure shows notable movements in loop regions such as the PEG-binding cavity and the β7–β8 loop. The residues from the PEG-binding cavity, in particular, moved closer together and the cavity size was reduced. The maximum movement, of approximately 1.2 Å, was found around Ala177. In the β7–β8 loop a maximum movement of approximately 2.6 Å was found around Gly205.

3.7. Modelling of substrate binding in the active site

The water molecules found in the active site form a channel that leads to the surface of the protein. The entrance of the channel is flanked by residues from loop 249–257 on one side and residues from loop 238–243 on the opposite side. The narrowest point (~3.9 Å) occurs between the C^{α} atoms of Asp256 and Gly239. The positions of the water molecules were used as a guide for manual docking of the 3-hydroxybutyrate (3HB) trimer. The latter was oriented in such a way that it occupied most of the water positions found in the cavity (Fig. 4). In this way, the substrate can make interactions with surrounding residues to stabilize its position. The most notable interactions include those of O3B with Gly164 N (3.3 Å), of O1A with Gly239 O (2.57 Å) and Cys255 O (3.06 Å) and of O1B with Gly163 O (2.73 Å) and Ala162 O (3.34). Additionally, O1M interacts with main-chain atoms from the 256–258 region of the protein surface.

4. Discussion

The crystal structures of free PhaZ7 and of the PhaZ7–SO_2 complex were determined at 1.45 and 1.2 Å resolution, respectively. Owing to the high resolution, both structures refined with good geometry and crystallographic statistics. The low difference between R_{cryst} and R_{free} indicates the correctness of the applied refinement strategy. The high-resolution structures allowed a better assignment of the secondary-structure elements. Three minor differences were identified compared with the lower (1.9 Å) resolution structure of PhaZ7. Overall, the structures confirmed the canonical α/β-hydrolase fold adopted by PhaZ7.

The active site of PhaZ7 is characterized by a Ser-His-Asp catalytic triad. The composition and arrangement of the catalytic triad in PhaZ7 are similar to those of serine proteases (Dodson & Wlodawer, 1998). The latter target a wide range of electrophilic (carbonyl) substrates by making a nucleophilic attack on them through the Ser residue. The nucleophilic potential around the seryl O atom is enhanced by hydrogen bonds to the backbone amide groups of neighbouring residues that form the oxyanion hole. The generated nucleophilic potential helps to attract electrophilic carbonyl compounds. In the absence of any substrate, a strong hydrogen bond is

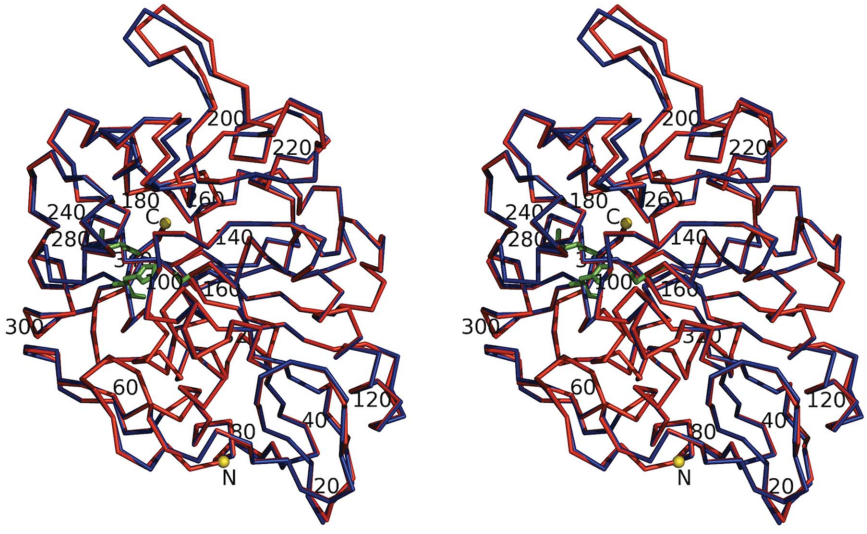

Figure 3
Stereoview of C^{α}-atom superposition of free PhaZ7 (PDB code 2vtv) and PhaZ7–SO_2. Free PhaZ7 is shown in red and PhaZ7–SO_2 is shown in blue. The C- and N-termini are shown as yellow spheres. The catalytic triad is depicted in green. Every 20th residue is numbered.

present between Ser OG and His NE2 (Perona & Craik, 1995; Carter & Wells, 1988). When a substrate is bound to Ser (tetrahedral intermediate), the hydrogen is transferred from Ser OG to His NE2, resulting in an increase in the positive charge on the imidazole ring of His (Warshel *et al.*, 1989; Frey *et al.*, 1994), which is then compensated by the carboxylate group of Asp forming two partial hydrogen bonds to one of the ring N atoms (Hedstrom, 2002). The same scenario applies in PhaZ7, as deduced from the PhaZ7–SO_2 structure. The SO_2 molecule was found to be tightly bound at the active site between Ser136 and His306 (Fig. 2), mimicking the tetrahedral intermediate. The observed distances of the S atom of SO_2 from Ser136 OG and His306 NE2 (1.43 and 1.64 Å, respectively) and the continuous electron density suggest covalent binding. The formation of a bond between the S atom of SO_2 and His306 NE2 results in an increase in the positive charge on the imidazole ring of His306, which is compensated by the carboxylate group of Asp242 through two partial hydrogen bonds to His306 ND1.

The PhaZ7–SO_2 structure also provides insight into the oxyanion-hole residues. One of them is Met137, based on the hydrogen bond formed between Ser136 OG and Met137 N. This is in agreement with the general notion that the residue following the nucleophile in the primary sequence contributes to the formation of the oxyanion hole (Nardini & Dijkstra, 1999). Moreover, the hydrogen bond between the O2 atom of SO_2 and Asn49 N implicates Asn49 as the second contributor to oxyanion-hole formation.

PMSF is an irreversible serine protease inhibitor. It inhibits serine proteases by sulfonating the serine residue at the active site and producing an inactive monosulfonyl enzyme (Gold & Fahrney, 1964; Gold, 1967). PMSF is an unstable molecule and may be hydrolyzed to benzylsulfinic acid (PMS) during use. Hence, cocrystallization with PMSF usually results in PMS bound at the active site, as found in a number of crystal structures [for example, PDB entries 1eq9 (Botos *et al.*, 2000), 1aur (Kim *et al.*, 1997), 1pqa (Schmidt *et al.*, 2003), 1klt (McGrath *et al.*, 1997), 1wpr (Kaneko *et al.*, 2005) and 2cbg (Samel *et al.*, 2006)]. Since only the SO_2 moiety was located in the catalytic cavity, its existence could be explained as an impurity in or a degradation product of the PMSF solution used in the cocrystallization. Interestingly, inhibitor studies in solution have shown that PhaZ7 retains 90% of its activity in the presence of 10 m*M* PMSF (Handrick *et al.*, 2001). The structure of PhaZ7 shows that the active site is buried and an aromatic ring such as that of PMSF cannot be accommodated without major structural rearrangements. Indeed, modelling of an entire PMS molecule based on the position of SO_2 resulted in severe clashes with His306. Thus, the lack of considerable inhibition by PMSF in solution is in agreement with our structural findings since PMSF cannot enter the active site for sulfonation and the arrangement of the catalytic residues does not favour its binding. In other depolymerases, such as the extracellular polyhydroxybutyrate depolymerase from *Thermus thermophilus* HB8, the inhibition is 90% at 10 m*M* PMSF, suggesting a solvent-accessible active site (Papaneophytou *et al.*, 2009).

Two surface-loop regions, namely the PEG-binding cavity and the polypeptide stretch Gly201–Ser209 between the β7 and β8 strands, are flexible and able to undergo conformational changes. These two regions are found at the monomer–monomer interface in the PhaZ7 dimer. It can be inferred from the superimposition that these two regions may facilitate proper binding of the polymer by changing their position owing to their susceptibility to conformational changes. However, the exact mechanism and binding mode of the biopolymer are still unknown and further studies are required.

The water molecules in the active site are arranged in a specific orientation. Docking studies using the 3HB trimer revealed a remarkable overlapping of water molecules with the substrate atoms, suggesting a plausible orientation of the substrate in the cavity. Accordingly, substrate binding would lead to replacement of these water molecules. Interestingly, the modelling further suggests that interactions within the cavity involve main-chain atoms, especially those from Gly and Ala residues, possibly preserving the specificity of the site. Moreover, sufficient space is available in the cavity near Ser136 to accommodate an extra substrate unit. This place might in fact be reserved for the hydrolysis product of the substrate.

In the current PhaZ7 structure the active site is inaccessible. The docking experiment is therefore in agreement with our previous proposal that major conformational changes are required to open up access to the active site. The orientation of the modelled substrate points to surface loops 249–257 and 238–243 as potential gatekeepers of the active site. It is noteworthy that the active sites of the other two depolymerases are in surface crevices and are readily available for polyester binding. In *Pe. funiculosum* e-PHB depolymerase no conformational changes were observed upon binding of the 3HB trimer substrate. Thus, different mechanisms may operate in depolymerases.

5. Conclusions

The crystal structure of *P. lemoignei* PhaZ7 depolymerase in complex with SO_2 was determined at 1.2 Å resolution and is currently the

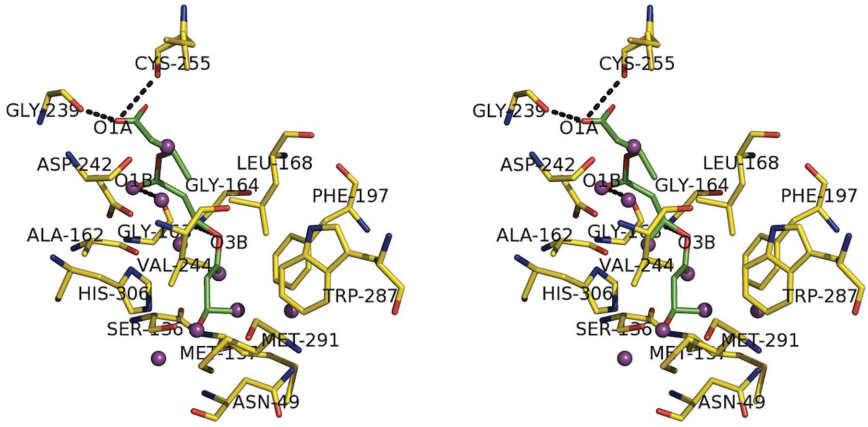

Figure 4
Docking of the 3HB trimer in the catalytic cavity (in stereo). The residues forming the catalytic cavity are shown as yellow sticks. The 3HB trimer is depicted as green sticks. The water molecules are shown as magenta spheres.

highest resolution depolymerase structure to be obtained. The structure showed binding of SO_2 in the active site and no significant conformational changes and hence confirms the presence of a pre-formed serine protease catalytic triad. Furthermore, the structure clearly established Met137 and Asn49 as the oxyanion-hole residues. The active site is deeply buried and inaccessible to the substrate in the present structure. Comparison with the free PhaZ7 structure in two crystal forms showed no significant differences in the vicinity of the active site. However, conformational changes were identified in surface loops, suggesting flexibility and possible involvement of these loops in polyester binding. Nine water molecules that form a channel leading to the surface of the structure were located in the active site. Based on the position of the water molecules, molecular docking revealed the binding mode for the substrate and displacement of the water molecules upon substrate binding. A closed–open–closed switch in the conformation of PhaZ7 in the presence of substrate is therefore suggested. Further studies with suitable substrate analogues and enzyme variants should provide full mechanistic details.

This work was supported by the Academy of Finland (Grant No. 121278 to ACP), the Finnish National Graduate School in Informational and Structural Biology (SW) and the Carl Zeiss Stiftung (SH). We thank the staff of the European Synchrotron Radiation Facility (ESRF), Grenoble, France and Teemu Haikarainen for help with data collection. Access to ESRF, Grenoble, France (European Commission Research Infrastructure Action under the FP6 'Structuring the European Research Area Specific Programme' contract No. RII3-CT-2004-506008) is gratefully acknowledged.

References

Abe, T., Kobayashi, T. & Saito, T. (2005). *J. Bacteriol.* **187**, 6982–6990.
Botos, I., Meyer, E., Nguyen, M., Swanson, S. M., Koomen, J. M., Russell, D. H. & Meyer, E. F. (2000). *J. Mol. Biol.* **298**, 895–901.
Carter, P. & Wells, J. A. (1988). *Nature (London)*, **332**, 564–568.
Chen, H. J., Pan, S. C. & Shaw, G. C. (2009). *Appl. Environ. Microbiol.* **75**, 5290–5299.
Chen, V. B., Arendall, W. B., Headd, J. J., Keedy, D. A., Immormino, R. M., Kapral, G. J., Murray, L. W., Richardson, J. S. & Richardson, D. C. (2010). *Acta Cryst.* D**66**, 12–21.
Collaborative Computational Project, Number 4 (1994). *Acta Cryst.* D**50**, 760–763.
Cruickshank, D. W. J. (1999). *Acta Cryst.* D**55**, 583–601.
Diederichs, K. & Karplus, P. A. (1997). *Nature Struct. Biol.* **4**, 269–275.
Dodson, G. & Wlodawer, A. (1998). *Trends Biochem. Sci.* **23**, 347–352.
Emsley, P. & Cowtan, K. (2004). *Acta Cryst.* D**60**, 2126–2132.
Frey, P. A., Whitt, S. A. & Tobin, J. B. (1994). *Science*, **264**, 1927–1930.
Gold, A. M. (1967). *Methods Enzymol.* **11**, 706–711.
Gold, A. M. & Fahrney, D. (1964). *Biochemistry*, **3**, 783–791.
Handrick, R., Reinhardt, S., Focarete, M. L., Scandola, M., Adamus, G., Kowalczuk, M. & Jendrossek, D. (2001). *J. Biol. Chem.* **276**, 36215–36224.
Hedstrom, L. (2002). *Chem. Rev.* **102**, 4501–4524.
Hiraishi, T., Hirahara, Y., Doi, Y., Maeda, M. & Taguchi, S. (2006). *Appl. Environ. Microbiol.* **72**, 7331–7338.
Hisano, T., Kasuya, K., Tezuka, Y., Ishii, N., Kobayashi, T., Shiraki, M., Oroudjev, E., Hansma, H., Iwata, T., Doi, Y., Saito, T. & Miki, K. (2006). *J. Mol. Biol.* **356**, 993–1004.
Jendrossek, D. (1998). *Polym. Degrad. Stab.* **59**, 317–325.
Jendrossek, D. (2001). *Adv. Biochem. Eng. Biotechnol.* **71**, 293–325.
Jendrossek, D. (2002). *Biopolymers*, edited by Y. Doi & A. Steinbüchel, pp. 41–83. Weinheim: Wiley-VCH.
Jendrossek, D. (2009). *J. Bacteriol.* **191**, 3195–3202.
Jendrossek, D. & Handrick, R. (2002). *Annu. Rev. Microbiol.* **56**, 403–432.
Jendrossek, D., Schirmer, A. & Schlegel, H. G. (1996). *Appl. Microbiol. Biotechnol.* **46**, 451–463.
Kabsch, W. (2010). *Acta Cryst.* D**66**, 125–132.
Kaneko, T., Tanaka, N. & Kumasaka, T. (2005). *Protein Sci.* **14**, 558–565.
Kapetaniou, E. G., Braaz, R., Jendrossek, D. & Papageorgiou, A. C. (2005). *Acta Cryst.* F**61**, 479–481.
Kim, K. K., Song, H. K., Shin, D. H., Hwang, K. Y., Choe, S., Yoo, O. J. & Suh, S. W. (1997). *Structure*, **5**, 1571–1584.
Kleywegt, G. J. & Jones, T. A. (1994). *Acta Cryst.* D**50**, 178–185.
Krissinel, E. & Henrick, K. (2004). *Acta Cryst.* D**60**, 2256–2268.
Krissinel, E. & Henrick, K. (2007). *J. Mol. Biol.* **372**, 774–797.
Madison, L. L. & Huisman, G. W. (1999). *Microbiol. Mol. Biol. Rev.* **63**, 21–53.
McCoy, A. J., Grosse-Kunstleve, R. W., Adams, P. D., Winn, M. D., Storoni, L. C. & Read, R. J. (2007). *J. Appl. Cryst.* **40**, 658–674.
McGrath, M. E., Mirzadegan, T. & Schmidt, B. F. (1997). *Biochemistry*, **36**, 14318–14324.
Merritt, E. A. (1999). *Acta Cryst.* D**55**, 1997–2004.
Miyazaki, S., Takahashi, K., Shiraki, M., Saito, T., Tezuka, Y. K. & Kasuya, K. (2002). *J. Polym. Environ.* **8**, 175–182.
Murshudov, G. N., Vagin, A. A. & Dodson, E. J. (1997). *Acta Cryst.* D**53**, 240–255.
Nardini, M. & Dijkstra, B. W. (1999). *Curr. Opin. Struct. Biol.* **9**, 732–737.
Papageorgiou, A. C., Hermawan, S., Singh, C. B. & Jendrossek, D. (2008). *J. Mol. Biol.* **382**, 1184–1194.
Papaneophytou, C. P., Pantazaki, A. A. & Kyriakidis, D. A. (2009). *Appl. Microbiol. Biotechnol.* **83**, 659–668.
Perona, J. J. & Craik, C. S. (1995). *Protein Sci.* **4**, 337–360.
Pötter, M. & Steinbüchel, A. (2005). *Biomacromolecules*, **6**, 552–560.
Reinhardt, S., Handrick, R. & Jendrossek, D. (2002). *Biomacromolecules*, **3**, 823–827.
Saito, T., Suzuki, K., Yamamoto, J., Fukui, T., Miwa, K., Tomita, K., Nakanishi, S., Odani, S., Suzuki, J. & Ishikawa, K. (1989). *J. Bacteriol.* **171**, 184–189.
Samel, S. A., Wagner, B., Marahiel, M. A. & Essen, L. O. (2006). *J. Mol. Biol.* **359**, 876–889.
Schmidt, A., Jelsch, C., Ostergaard, P., Rypniewski, W. & Lamzin, V. S. (2003). *J. Biol. Chem.* **278**, 43357–43362.
Sheldrick, G. M. (2008). *Acta Cryst.* A**64**, 112–122.
Steinbüchel, A. & Valentin, H. E. (1995). *FEMS Microbiol. Lett.* **128**, 219–228.
Warshel, A., Naray-Szabo, G., Sussman, F. & Hwang, J. K. (1989). *Biochemistry*, **28**, 3629–3637.